EnvironmentAsia
The international journal by the Thai Society of Higher Education Institutes on Environment

EnvironmentAsia 16(3) 2023 68-81
DOI 10.14456/ea.2023.36
ISSN 1906-1714; ONLINE ISSN: 2586-8861

Assessment of Solar Rooftop Potential Using a Digital Surface Model Based on a Photogrammetric Survey by an Unmanned Aerial Vehicle

Warin Wongwan[1], Narong Pleerux[1*], Nattapan Thanomsat[2], and Sitthisak Moukomla[3]

[1]Faculty of Geoinformatics, Burapha University, Chonburi, Thailand
[2]Department of Electrical Engineering, Faculty of Engineering, Burapha University, Chonburi, Thailand
[3]Geo-Informatics and Space Technology Development Agency (GISTDA), Bangkok, Thailand

*Corresponding author: narong_p@buu.ac.th
Received: May 8, 2023; Revised: June 28, 2023; Accepted: July 21, 2023

Abstract

The Digital Surface Model (DSM) provides significant input data for solar radiation analysis. The DSM data for a small area like a university can be obtained from Unmanned Aerial Vehicle (UAV) photogrammetric surveys. This method has the advantages of being low cost and less time consuming while also having high-resolution and accurate results. This study analyzed solar radiation with Point Solar Radiation analysis tools from the ArcGIS software. A rooftop solar radiation map was derived and used for identifying potential buildings for installing photovoltaic (PV) systems and to estimate the PV value. Most of the PV-potential areas consisted of structured buildings with flat and pitched roofs covering 10.2% of the rooftop area. The pitched roofs were oriented toward the south and not over a 40° slope. PV values estimated from the installed PV systems were compared with the actual PV values. The estimated values were higher than the actual values by 0.19%. The potential PV area was analyzed by comparing the estimated PV value with the university's electricity demand. It was estimated that the installation of PV systems in the potential PV areas could reduce electricity costs by up to 42.28%. Solar radiation analysis and potential PV assessment can provide supportive information on the financial feasibility and estimated power cost savings that would accrue on installing rooftop PV systems in buildings and help in decision making.

Keywords: Solar radiation; Solar rooftop; Photovoltaic (PV); Digital Surface Model (DSM); Geographic Information System (GIS)

1. Introduction

The university under study was a large academic institution that consumed a large amount of power; the air conditioning system consumed 40% – 60% of the power, the lighting consumed 10% – 30%, and other devices like computer, monitor, photocopier, elevator, etc. consumed 5% – 20% (Ministry of Energy, 2007). The power costs were significant, and there was a need to reduce them. The power costs can be reduced by not only reducing the power consumption but also by installing PV systems on the institute's rooftops. The power generated by PV systems is in synchronization with the demand which is more during the day and less at night. For this study area, Lampang Rajabhat University (LPRU) has an average monthly power consumption of 300,418 kWh. In 2021, a rooftop PV system with a capacity of 300 kW was installed, along with a policy

aimed at reducing power consumption. These initiatives collectively led to a reduction in power costs by 5.26%. However, there is still a considerable amount of available roof area that can be utilized for the installation of additional PV systems.

The rooftops of buildings are valuable resources for generating solar power, but the potential is limited by the shadows from surrounding buildings and trees and building orientation (Boccalatte *et al.,* 2022; Han *et al.,* 2019). However, the amount of power generated largely depends on the availability of annual solar radiation more than on the aforementioned factors (Moudrý *et al.,* 2019). In recent years, advancements in PV technology have led to higher efficiency with lower area requirements, higher power output, and lower costs. These advancements encourage the installation of rooftop PV systems in academic institutes that have high power consumption with associated high power costs and show a trend of increasing power consumption over time. However, the amount of power generated from the PV systems varies with solar radiation, and an analysis of solar radiation is needed to identify high potential buildings and determine the feasibility of investment in rooftop PV systems.

The solar energy potential of rooftops has been assessed in many countries using various methods, with the geographic information system (GIS) being an important tool for this assessment (Huang *et al.,* 2022). The use of GIS for solar radiation analysis requires the application of the digital elevation model or the DSM as the topography affects the solar radiation potential. The DSM is based on topography survey using light detection and ranging or UAV technology. UAVs have a limitation; they cannot survey large areas as they have short flight times due to limited battery capacity and a short remote control range (Yalcin, 2018). However, UAVs have always been used for photogrammetric surveys of small areas for generating DSMs with high accuracy, high-resolution, and low cost (Bilasco *et al.,* 2022). The solar radiation analysis tools available in ArcGIS were initially developed in year 2000 (Fu and Rich, 2000). Since then, these models have been widely utilized to assess solar radiation on rooftops in various areas, including urban and rural regions. Several studies have used DSM data for the analysis of solar radiation on rooftops (Kodysh *et al.,* 2013; Pili *et al.,* 2018; Kazak *et al.,* 2018). The results enabled identification of high potential buildings for rooftop PV system installation. The validity and reliability of solar radiation analysis tools were evaluated by comparing the assessment of solar potential on rooftops with actual solar radiation measurements obtained through a solar radiation meter (Suomalainen *et al.,* 2017). The solar energy potential on the roof of a building was estimated prior to the installation of solar panels and was then compared with the actual data recorded after the installation of the panels to evaluate the reliability and performance of the estimation methods used (Fuentes, 2020).

The objective of this study was to assess the solar rooftop potential at LPRU based on DSM from UAV. The PV value was estimated for the areas with PV installation and checked against the actual PV value obtained from the meter readings. This approach helped assess the solar rooftop potential in terms of the electricity generated. The results of this study can be used to justify the installation of rooftop PV systems in other buildings within LPRU thereby reducing the power costs and fossil fuel consumption and promoting sustainable energy while reducing CO_2 emission to Net Zero Emission GHGs.

2. Materials and methods

This method for estimating the solar energy potential with ArcGIS solar analysis tool based on DSM from UAV data facilitates the creation of solar radiation maps on rooftops with high precision. These tools are integrated into the above workflow to analyze the solar radiation potential of a specific area. In this work, the solar energy potential of the method is compared against the real performance obtained from the solar PV system installed in the study area. Figure 1 shows a flowchart of the method performed in this work.

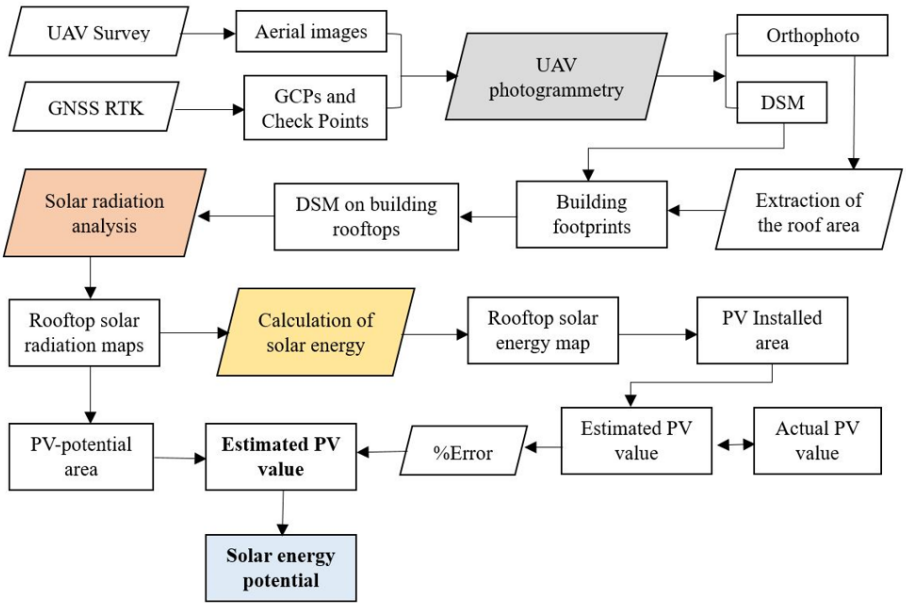

Figure 1. Flowchart of assessment of solar rooftop potential

2.1 The UAV photogrammetric survey

Aerial imagery was obtained using a DJI Phantom 3 Professional UAV equipped with an FC300X (3.61 mm) camera with 4000×3000-pixel resolution. Specifically, flights were executed with 80% along-track overlap and 80 % cross-track overlap. The UAV-based aerial photography produced high-resolution (0.1 m) DSM with high accuracy. 20 autopilot missions over an LPRU area (18°13'27" N to 18°14'27" N latitude and 99°28'27" E to 99°29'32" E longitude) of 2.35 km^2 produced 2,253 aerial images. A data processing procedure was executed with the preinstalled GCPs in Agisoft PhotoScan Professional software, running on a Windows 10, with a 16-core AMD Ryzen 9 3950X processor, 64 GB RAM, 5 GB NVIDIA Quadro P2000 video card. The positions of 12 GCPs and 26 Check Points were marked and measured with a portable GNSS CHC i80 receiver. A Real Time Kinematic (GNSS RTK) receiver can provide positioning information to centimeter-level accuracy and further enhance the accuracy of the output model (Abdollahnejad *et al.,* 2018). After GCP establishment, flight operations, and data processing, a georeferenced orthophoto and a DSM with a ground sampling distance of 5.06 cm/pixel were produced as shown in Figure 2, and the processing time was 29 hours 10 minutes. The localization accuracy (RMSE) of the model was determined as 9.95 cm and 13.05 cm for the horizontal and vertical planes, respectively, as shown in Table 1. This high-resolution DSM can be used as an input to solar radiation analysis tools.

2.2 Extraction of the roof area

The roof area represents the building footprint. Using the rooftop edges to define polygons for each building and represent the outline of a given building. The building footprint approach involved manually digitizing the roof outlines. 7 LPRU buildings had installed PV panels, and the other buildings did not, as shown in Figure 3(a). The roof DSM, created using building footprints, can be used as input to solar radiation analysis tools as shown in Figure 3(b).

2.3 Calculation of the solar radiation

The solar radiation analysis tools in the ArcGIS Spatial Analyst extension calculate radiation across a landscape or for specific locations, based on methods from the hemispherical viewshed algorithm developed by Rich *et al.,* (1994) and further developed by Fu and Rich (2000).

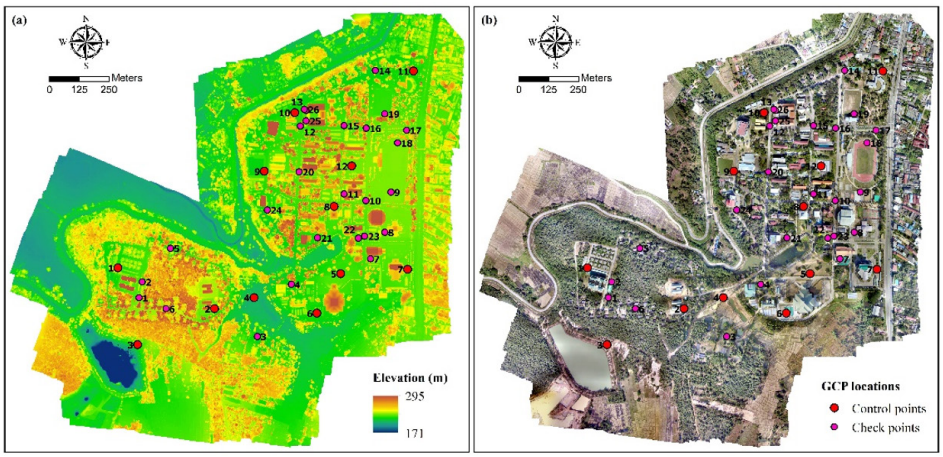

Figure 2. Results of the topographic survey in LPRU: (a) DSM and (b) Orthophoto

Table 1. Control points and check points RMSE

X error (cm)	Y error (cm)	Z error (cm)	XY error (cm)	Total (cm)	Image (pix)
12 GCPs					
1.19498	1.4352	0.378067	1.86755	1.90544	0.132
26 Check Points					
6.7107	7.35172	13.0484	9.95396	16.4116	0.229

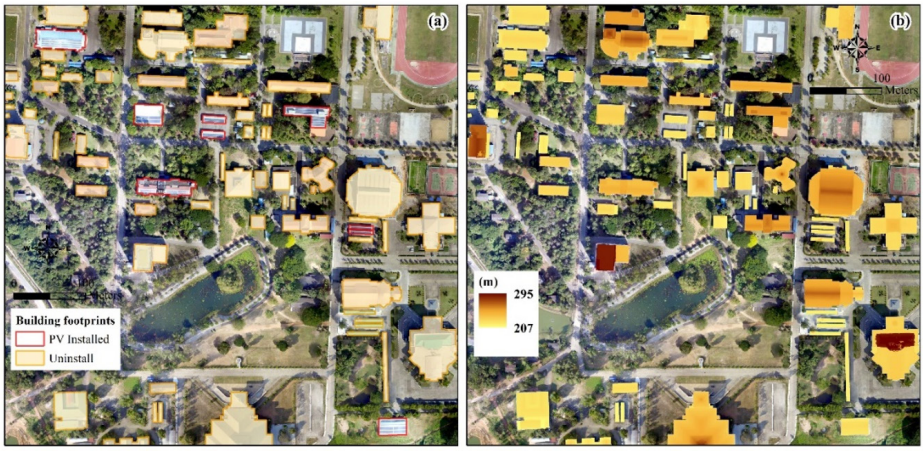

Figure 3. (a) Building footprints and (b) DSM on building rooftops

Highly optimized algorithms account for influences of the upward–looking viewshed, surface orientation, elevation, and atmospheric conditions. Since radiation can be greatly affected by topography and surface features, a key component of the calculation algorithm requires the generation of an upward-looking hemispherical viewshed for every location in the digital elevation model (DEM). The solar radiation tool consists of the following calculations:

2.3.1 Viewshed calculation

The viewshed is a raster representation of the entire sky that is visible or obstructed when viewed from a particular location. A viewshed is calculated by searching in a specified number of directions around a location of interest and determining the maximum angle of sky obstruction, or horizon angle. For all other unsearched directions, horizon angles are interpolated. Horizon angles are then

converted into a hemispherical coordinate system, thus representing a three-dimensional hemisphere of directions as a two-dimensional raster image. Each raster cell of the viewshed is assigned a value that corresponds to whether the sky direction is visible or obstructed. Output cell locations (row and column) correspond to zenith angle θ (angle relative to straight upward) and azimuth angle α (angle relative to north) on the hemisphere of directions.

Viewsheds are used in conjunction with sun position and sky direction information (represented by a sun map and sky map, respectively) to calculate direct, diffuse, and total (direct + diffuse) radiation for each location and to produce an accurate radiation map.

2.3.2 Sun map calculation

The direct solar radiation originating from each sky direction is calculated using a sun map in the same hemispherical projection as the viewshed. A sun map is a raster representation that displays the sun track, or apparent position of the sun as it varies through the hours of day and through the days of the year. The sun map consists of discrete sectors defined by the sun's position at particular intervals during the day (hours) and time of year (days or months). The sun tracking is calculated based on the latitude of the study area and the time configuration that defines sun map sectors. For each sun map sector, a unique identification value is specified, along with its centroid zenith and azimuth angle. The solar radiation originating from each sector is calculated separately, and the viewshed is overlaid on the sun map for the calculation of direct radiation.

2.3.3 Sky map calculation

Diffuse radiation originates from all sky directions as a result of scattering by atmospheric components (clouds, particles, and so forth). To calculate diffuse radiation for a particular location, a sky map is created to represent a hemispherical view of the entire sky divided into a series of sky sectors defined by zenith and azimuth angles. Each sector is assigned a unique identifier value, along with the centroid zenith and azimuth angles. Diffuse radiation is calculated for each sky sector based on direction (zenith and azimuth).

2.3.4 Solar radiation calculation

After obtaining the calculations of the viewshed, the sun map, and the sky map, this information is taken to calculate the diffuse and direct radiation received by the elevation model. The total solar radiation or global solar radiation (*Rad_Glob*) is calculated as the sum of the direct (*Rad_Dir*) and diffuse solar radiation (*Rad_Dif*) of all sectors of the sun map and the sky map. This calculation takes into account the position of the sun, the attenuation of the atmosphere, and how the topographic reception surface is oriented. The result is a solar radiation map for the entire area of interest, as illustrated in Equation (1)

$$Rad\_Glob = Rad\_Dir + Rad\_Dif \quad (1)$$

The total direct radiation (*Rad_Dir*) for a given location is the sum of the direct insolation (*Dir*) of a sector of the sun map with a centroid at the zenith angle θ and azimuth angle α as expressed in Equation (2)

$$Rad\_Dir = \sum Dir\ \theta, \alpha \quad (2)$$

The total diffuse solar radiation (*Rad_Dif*) for a given location is the sum of the diffuse radiation (*Dif*) of a sector of the sun map with a centroid in the zenith angle θ and azimuth angle α, as illustrated in Equation (3):

$$Rad\_Dif = \sum Dif\ \theta, \alpha \quad (3)$$

Direct radiation is calculated using Equation (4):

$$Dir = ConS \times \beta m(\theta) \times SolDur\theta, \alpha \times SolGap\theta, \alpha \times \cos(AngIn\theta, \alpha) \quad (4)$$

Where *ConS* is the solar constant and has a value of 1.367 kW/m^2; β is the transmissivity of the atmosphere for the shortest path in the zenith direction; $m(\theta)$ is the relative optical path length; $SolDur\theta,\alpha$ is the time duration represented by the sky factor; $SolGap\theta,\alpha$ is the gap fraction for the sun map sector; and

AngInθ,α is the angle of incidence between the centroid of the sky sector and the axis normal to the surface.

Diffuse radiation (*Diff*) is calculated using Equation (5):

$$Dif = Rglo \times Pfr \times Dur \times SkyGap\theta,\alpha \times Weight\theta,\alpha \times \cos(AngIn\theta,\alpha) \quad (5)$$

Where *Rglo* is the global normal solar radiation; *Pfr* is the proportion of global normal solar radiation flux that is diffused; Dur is the time interval for analysis; *SkyGapθ, α* is the gap fraction (proportion of visible sky) for the sky sector; *Weightθ, α* is proportion of diffuse radiation originating in a given sky sector relative to all sectors; and *AngInθ, α* is the angle of incidence between the centroid of the sky sector and the intercepting surface.

Atmospheric conditions such as cloud cover, precipitation, dust, and others can significantly decrease the amount of diffuse and direct solar radiation reaching a surface. The approach adopted in this model. Transmittivity is a property of the atmosphere and is the ratio of the energy received at the upper edge of the atmosphere to that reaching the earth's surface by the shortest path (in the direction of the zenith). Values range from 0 (no transmission) to 1 (complete transmission). Typically, observed values are 0.6 or 0.7 for very clear sky conditions and 0.5 for a generally clear sky.

In the solar radiation model, it was possible to set model parameters to account for site-specific variables that impacted solar radiation levels for a particular location, such as transmittivity values (clear sky) and time of year (the whole year with monthly intervals). The calculation of the solar radiation was based on the Point Solar Radiation tool in ArcGIS 10.3, which was used by DSM to generate the aspect map and slope map, which, along with specific locations in a point feature class or location table, contribute to the calculation of the solar radiation value for the pixels in the DSM. The calculations for finding the sum and average of pixels in the area of interest on the rooftops, in the PV installed and PV-potential areas, were done by ArcGIS zonal statistics.

2.4 Calculation of solar energy

The raster calculator tool in ArcGIS was applied to create a series of monthly solar energy data using the refined solar radiation data from the building rooftop map. Formula (7) was employed to estimate the electrical energy produced by the PV system (Pop *et al.,* 2021).

$$E = A \times R \times H \times PR \quad (7)$$

Where *E* is produced energy in kWh, *A* is the total area of PV panels in m^2: in this simulation, it was the pixel area of 0.01 m^2 (0.1 m × 0.1 m), *H* is the average solar radiation on the PV panels in kWh/m^2: in this simulation, it was the solar radiation value of the pixels, *PR* (Performance ratio) is a very important value for evaluating the quality of a PV system because it guarantees performance regardless of the orientation or inclination of the panel. It includes all the loss coefficients (between 0.5 and 0.9). In this simulation, the conversion efficiency from DC to AC was considered as 85% (0.85), and R is the efficiency of the solar panel given by a ratio %; this ratio is given for Standard Testing Conditions: radiation = 1000 Watts/m^2, cell temperature = 25 °C, wind velocity = 1 m/s, AM = 1.5 in this simulation. The Solartron Solar Module SP320 solar panel was used at a maximum power (P_{max}) of 320 Watts, and the area of the solar panel was (length × width) 1.958 m^2. Using the formula (8), the efficiency of the solar panel was calculated as 16.34%

$$Efficiency\ (\%) = \left(\frac{P_{max}}{Area \times 1000}\right) \times 100\% \quad (8)$$

2.5 Calculation of the percentage error

In the PV installed area, the estimated solar energy was compared with the actual PV value from the meter readings as a percentage error (%error). Using the formula (9), the %error was calculated as the difference between the estimated and actual PV values in percentage. In the PV-potential area, the estimated solar energy was subtraction of the %error, the resulting estimated solar energy potential matched the actual value.

$$\%error = \left|\frac{estimated\ value - actual\ value}{actual\ value}\right| \times 100 \quad (9)$$

3. Results and discussion

This study presents a method for estimating the solar radiation values for multiple buildings in a small area, such as in a university. The method uses a high-resolution DSM taken from a UAV photogrammetric survey with a solar radiation model, which was a hemispherical viewshed algorithm to account for the unique variables that influence solar radiation potential in GIS. This method has been demonstrated to work effectively for creating building rooftop solar radiation maps of a small area.

3.1 Rooftop solar radiation maps

The output of the solar radiation analysis was a series of monthly rooftop solar radiation maps in LPRU from January to December 2021. The annual total of solar radiation on the rooftops (given in kWh/m^2) was in the range of 234.25 – 1810.53 kWh/m^2, as shown in Figure 4. To achieve maximum efficiency in generating electricity, PV panels in Thailand should be oriented towards the south to receive continuous solar radiation throughout the day. In contrast, the north direction receives the least solar radiation. East and west directions receive moderate amounts. However, solar intake is limited for panels facing east or west, primarily in the morning until noon, resulting in reduced panel capacity. This information aligns with the solar radiation map, which also indicates that roofs with high slopes can have an impact on the amount of solar radiation received.

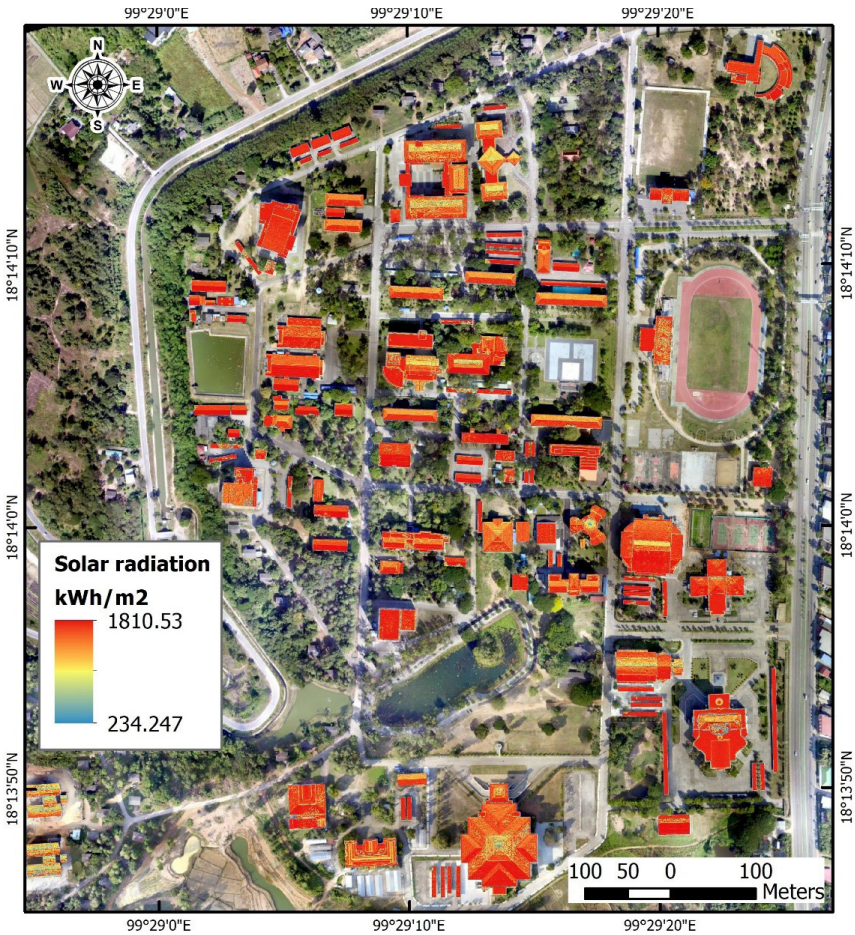

Figure 4. Rooftop solar radiation map of LPRU in 2021

Figure 5 shows buildings in LPRU were divided into three types by roof structure: pitched roof, flat roof, and complex roof buildings. When identifying PV-potential areas on rooftops, consideration is given to high solar radiation and roof structure. The following guidelines apply: (1) For flat roof buildings with non-high solar radiation, solar panels should be oriented towards the south and inclined at a 15° angle for optimal efficiency. (2) Pitched roofs can have a part with a maximum tilt of 40°, preferably oriented towards the south or southeast to maximize solar exposure. (3) Complex roof buildings may have areas similar to the above guideline (2), where the available space is sufficient to accommodate at least 80 solar panels (capacity 25 kW). In such cases, installing a PV system becomes cost-effective. However, it is crucial to ensure that the PV-potential area is free from shadows caused by trees or other buildings, as this can affect the efficiency of the rooftop PV installation.

After conducting an analysis to identify areas with potential for PV system installation on rooftops, a total of 23 buildings were identified as suitable candidates. Among these, 16 buildings had pitched roofs, 5 buildings had flat roofs, and 2 buildings had complex roofs. The slope of the pitched roofs was measured at an average angle of 20.42°, while the complex roofs had a slope of 19.75°. The average monthly solar radiation on the flat roofs was 146.15 kWh/m^2, on the pitched roofs was 142.14 kWh/m^2, and on the complex roofs was 146.65 kWh/m^2.

Table 2 shows the rooftop solar radiation in three areas. 1) The rooftop area had an average monthly solar radiation of 130.69 kWh/m^2. The maximum solar radiation was 163.70 kWh/m^2 in July and the minimum was 87.10 kWh/m^2 in December. The annual total solar radiation was 1,568.34 kWh/m^2. 2) PV installed area: In 2017, LPRU installed PV systems on rooftops. 944 panels (size of panel 1.96 m^2) were installed. The total installed area was 1,836.74 m^2, and the annual total solar radiation was 1,722.03 kWh/m^2. 3) PV-potential area could install 5,050 more solar panels. The total potential area was 7,977.14 m^2, the average monthly solar radiation was 144.38 kWh/m^2, and the annual total solar radiation was 1,738.70 kWh/m^2. In conclusion, our analysis of the solar radiation of rooftops in the PV-potential area indicates that these values closely with the solar radiation observed in the PV installed area. This finding validates our successful identification of the PV-potential area.

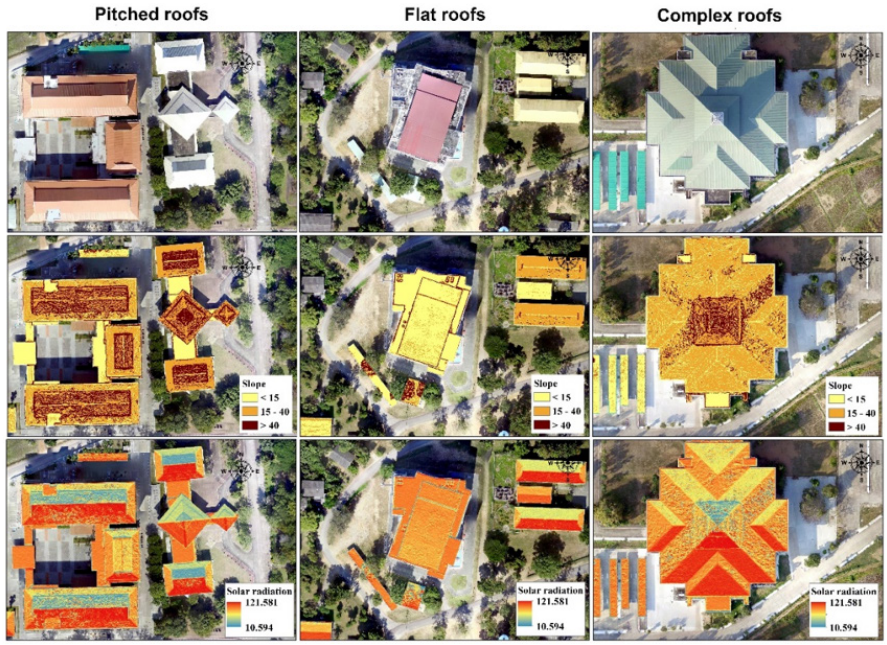

Figure 5. Slope and solar radiation on pitched, flat, and complex roofs

Table 2. Solar radiation on the rooftop area

Month	Solar radiation (kWh/m^2)		
	Rooftop area	PV installed area	PV-potential area
Jan	93.33	115.14	113.38
Feb	101.99	122.34	120.31
Mar	137.44	158.23	155.32
Apr	150.35	165.78	162.47
May	162.95	173.37	169.71
Jun	158.85	166.45	162.86
Jul	163.70	172.87	169.19
Aug	158.76	172.90	169.37
Sep	143.55	163.21	160.13
Oct	116.08	137.75	135.39
Nov	94.25	115.62	113.82
Dec	87.10	108.36	106.75
Monthly average	130.69	147.67	144.89
Yearly total	1,568.34	1,772.03	1,738.70
Area (m^2)	96,186.00	1,836.74	7,977.14

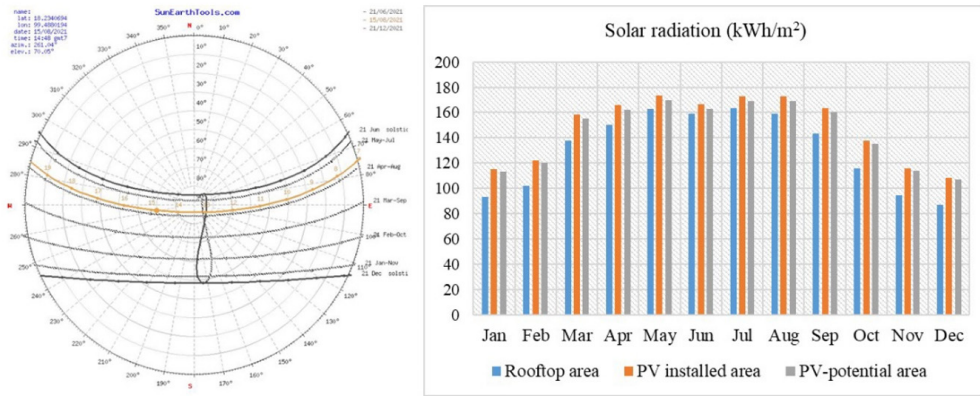

Figure 6. Analemma and solar radiation on the rooftop area of LPRU in 2021

The solar radiation on rooftop areas in year 2021 is shown in Table 2. It illustrates the variations in solar radiation resulting from the changing position of the sun in the sky throughout the year. This movement follows a pattern resembling the number 8, known as the analemma phenomenon, caused by the Earth's tilt of approximately 23.5°. In April, the sun aligns with the crossover of the number 8 and then moves northward, reaching its northernmost position during the summer solstice on June 21. Afterward, it starts moving southward, reaching the crossover of the number 8 again in August. During the winter solstice on December 21, the sun is at its southernmost position before returning to the north (Figure 6). The upper curve of the number 8, spanning from May to July, corresponds to the period when the North Pole faces the sun, representing the summer season with the highest solar radiation of the year. Conversely, the lower curve of the number 8, spanning from November to January, represents winter when the North Pole is turned away from the sun, resulting in the lowest solar radiation of the year.

3.2 Solar Energy Potential

The output of solar energy assessment was a series of monthly rooftop solar energy maps in LPRU. The annual total of solar energy on the rooftops (given in kWh) was the range of 0.326 – 2.515 kWh, as shown in Figure 7.

The total energy was calculated from the pixels in the PV installed area of the solar energy map (Figure 7). The annual total of estimated PV values was 452,716.38 kWh, and the monthly average was 37,726.37 kWh. In the same area in 2021, actual values obtained from meter readings for the PV installed area were 380,789.18 kWh, and 31,732.43 kWh for annual and monthly averages, respectively, as shown in Table 2. From the above result, it can be seen that the estimated PV value was more than the actual PV value by 0.19% (error). The estimated solar energy of the PV-potential area was the estimated PV value after subtraction of the %error.

Table 3 shows that May has the highest solar energy values for the PV Installed area (both actual and estimated) and estimated value of the PV-potential area, due to the higher solar radiation value compared to the other months (Table 2). Meanwhile, the error was more in the period June – October as it was the rainy season. The cloud cover affected the solar radiation, and therefore, PV systems generated less power (Figure 8). The error occurred because the solar radiation analysis was under clear sky conditions without regard to the atmospheric conditions especially the cloud cover of the area. For this reason, the estimated values were higher than the actual values.

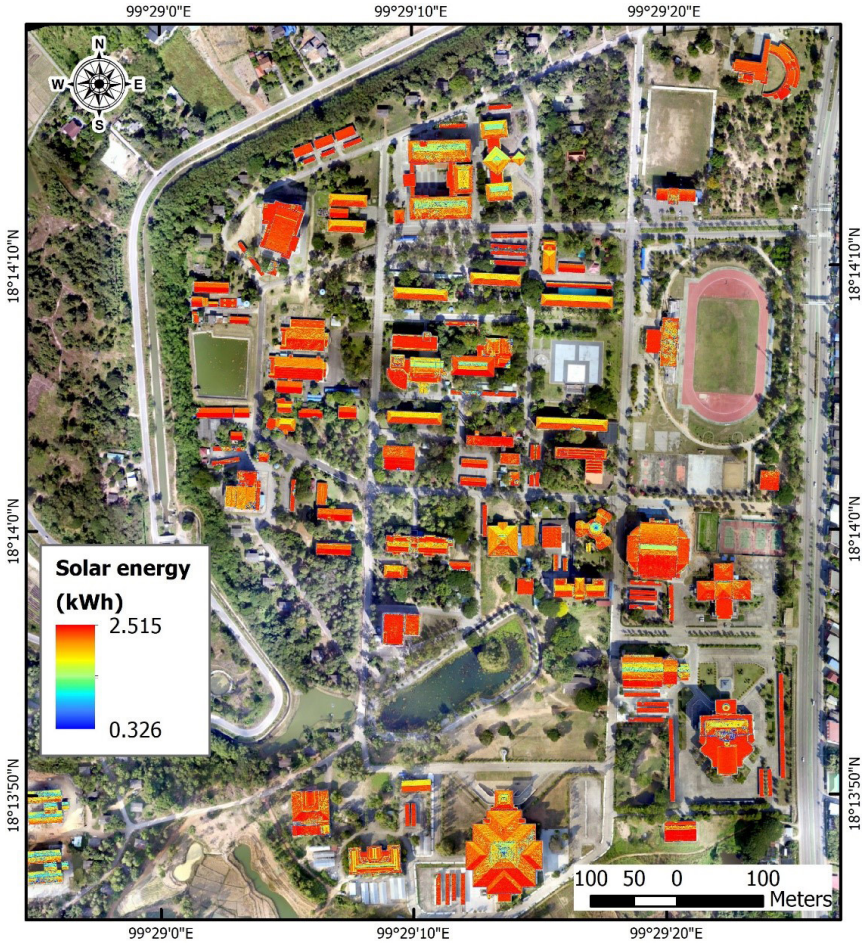

Figure 7. Rooftop solar energy map of LPRU in 2021

In solar energy calculations, the air mass value helps estimate the reduction in solar energy intensity due to factors such as absorption, scattering, and reflection by atmospheric components like gases, aerosols, and clouds. Air mass represents the distance sunlight travels through the earth's atmosphere to reach an observer on the ground. It is affected by the declination angle of the sun, which in turn depends on the sun's position in the sky. When the sun is directly overhead (at zenith), the air mass is minimal as the light takes a shorter path through the atmosphere, the air mass is considered to be 1. As the sun moves away from the zenith, the angle of incidence increases, and the air mass increases. When the sun is at an angle of 60° from the zenith, the air mass is approximately 2. The higher the air mass value, the longer the path length and the greater the atmospheric attenuation experienced by the sunlight. The air mass value of 1.5 is often used as a standard to estimate solar energy absorption and atmospheric effects on light propagation.

However, in order to the resulted estimated solar energy potential matched the actual PV value. Finally, the estimated solar energy of the PV-potential area was subtraction of the %error.

Table 3. Estimated solar energy of the PV Installed and PV-potential area

Month	PV Installed area			PV-Potential area
	Actual (kWh)	Estimated (kWh)	%Error	Estimated (kWh)
Jan	28,212.00	29,490.56	0.05	116,475.14
Feb	30,480.60	31,310.24	0.03	126,738.90
Mar	35,150.44	40,444.38	0.15	144,164.73
Apr	35,826.80	42,321.72	0.18	146,742.99
May	38,705.12	44,211.50	0.14	161,870.14
Jun	32,990.20	42,425.78	0.29	129,746.42
Jul	36,240.00	44,074.26	0.22	147,710.27
Aug	31,386.31	44,122.00	0.41	111,337.95
Sep	29,974.20	41,703.51	0.39	106,805.17
Oct	29,217.05	35,241.58	0.21	116,665.45
Nov	27,001.66	29,609.70	0.10	110,795.82
Dec	25,604.80	27,761.13	0.08	104,991.17
Monthly average	31,732.43	37,726.37	0.19	127,003.68
Yearly total	380,789.18	452,716.38	0.19	1,524,044.15

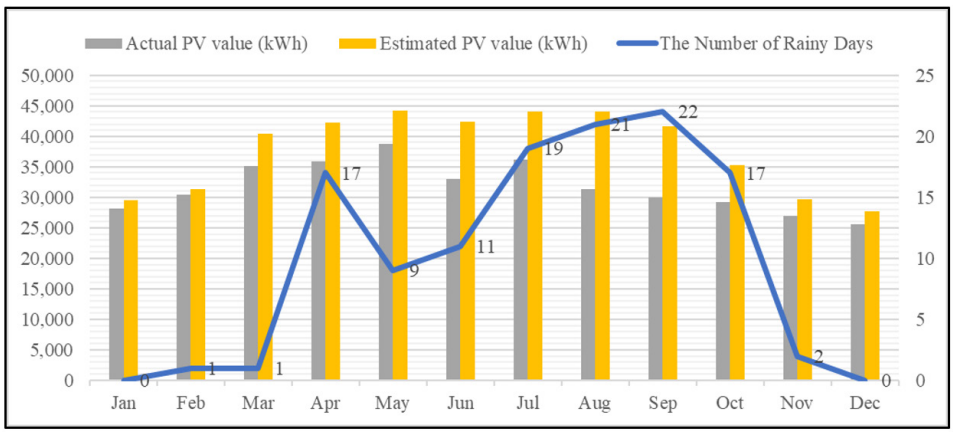

Figure 8. Number of rainy days in 2021, comparison of actual and estimated PV value of the PV Installed area

Figure 9. Solar energy potential of (a) PV installed and (b) PV-potential area

As derived from the PV-potential area (Figure 9), the annual total of the estimated PV value after subtraction of the %error was 1,524,044.15 kWh and the average monthly value was 127,003.68 kWh, as shown in Table 3. The average monthly electricity consumption was about 300,418.12 kWh. The installation of the PV system in the PV-potential area can reduce electricity costs by up to 42.28%.

3.3 Discussion

Solar radiation analysis must take into account the topography in DSM (Park *et al.,* 2016). Surface analysis of the topographic features, such as slope and aspect, generated from the DSM affect solar radiation, and help assess solar radiation efficiently (Cioban *et al.,* 2013). The DSM used for this study was generated from a UAV photogrammetric survey. It was a high accuracy and high-resolution DSM (0.1 m) and provided significant data input for solar radiation analysis, similar to studies (Yalcin, 2018; Bilasco *et al.,* 2022). The high-resolution DSM was used to assess solar radiation with Point Solar Radiation tools in the ArcGIS Spatial Analyst extension, was under clear sky conditions without regard to the weather of each area (Machete *et al.,* 2018)

The generated solar radiation map could identify the potential buildings for the installation of PV systems. The rooftop solar radiation map generated from solar radiation analysis showed the solar radiation potential obtained from pixels was better than the regional solar radiation average from the buildings. Solar radiation analysis showed that the annual total solar radiation of 1,568.34 kWh/m^2 was less than the long-term annual average for the period 2007 – 2018 from Solargis by 1,839.00 kWh/m^2. The results indicate that a suitable area for PV systems should have a maximum 40° slope, should be oriented toward the south or southeast, and be free of barriers and shadows of trees or buildings that may block the solar radiation. Rooftops that sloped more than 40° would get lesser solar radiation, thereby having a lower efficiency of power generation (Wong *et al.,* 2016). The solar radiation map helped identify the high potential buildings for PV system installation and helped decide the suitability based on the best orientation and slope without shadows from surrounding trees or buildings (Rodríguez *et al.,* 2017).

The assessment of solar rooftop potential compared the estimated PV value for the PV installed area with the actual PV value obtained from the meter readings. The estimated PV value was higher than the actual PV value with a 0.19% difference. The conclusion was that the estimated PV value closely matched the actual PV value. The difference occurred as the solar radiation analysis assumed a clear sky without considering the specific weather conditions in each area (especially temperature), which affected the amount of power generation (EKİCİ *et al.,* 2016).

The solar rooftop potentials were calculated only from the PV-potential area. If all the rooftop areas were included, it may lead to over or under estimation (Zhong *et al.,* 2022). In addition, it was found that the area exposed to high solar radiation would have high solar energy potential since the amount of electricity generated from the PV system varied with the solar radiation (Polo *et al.,* 2015).

4. Conclusion

The high-resolution DSM generated from the UAV photogrammetric survey, along with the solar radiation analysis tools in the ArcGIS, provided significant data for the assessment of solar radiation on building rooftops under clear sky conditions. Rooftop solar radiation maps were used to assess the rooftop solar energy potential, and that, in turn, helped identify the part of the rooftops with high solar energy potential. This study found that 10.2% of rooftop areas had a high potential for solar power generation. On flat roof structures, solar panels could be installed to cover all areas except the barrier area. On pitched roofs, the panels could be installed only on the sloping areas oriented to the south and with a tilt of 40° maximum. Complex rooftops were not conducive to solar power generation. These points should be taken into account in new buildings to ensure that the roof structures, slopes, and orientations support PV system installation and solar power generation.

The solar rooftop potential was confirmed by comparing the estimated PV value with the actual value. The estimated PV value was higher than the actual PV value by 0.19%. The difference arose because the cloud cover was not accounted for in the analysis. However, these are important factors affecting solar power generation. When the difference was subtracted from the estimated PV, the resulting solar potential assessment matched the actual. This estimated solar potential is vital for decision making about the installation of rooftop PV systems and provides an opportunity to reduce power consumption costs. This study introduces a method for estimating solar radiation on building rooftops, improving upon previous approaches. The method generates rooftop solar radiation maps using a formula to estimate electrical energy generation from photovoltaic (PV) systems. The accuracy of the estimations was validated by comparing them to actual data, revealing significant improvements in the estimation values.

Future research should be considering the impact of cloud cover, as it affects the amount of solar radiation reaching the PV panels, and temperature, which can influence the efficiency of the PV system.

Acknowledgement

Thank you very much to Lampang Rajabhat University for facilitating to gathering and providing essential data for this research.

References

Abdollahnejad A, Panagiotidis D, Surový P, Ulbrichová I. UAV Capability to Detect and Interpret Solar Radiation as a Potential Replacement Method to Hemispherical Photography. Remote sensing 2018; 10: 423.

Bilasco S, Hognogi G, Rosca S, Pop A, Iuliu V, Fodorean I, Marian-Potra A, Sestras P. Flash Flood Risk Assessment and Mitigation in Digital-Era Governance Using Unmanned Aerial Vehicle and GIS Spatial Analyses Case Study: Small River Basins. Remote Sensing 2022; 14: 2481.

Boccalatte A, Thebault M, Ménézo C, Ramousse J, Fossa M. Evaluating the impact of urban morphology on rooftop solar radiation: A new city-scale approach based on Geneva GIS data. Energy and Buildings 2022; 260: 111919.

Cioban A, Criveanu H, Matei F, Pop I, Rotaru A. Aspects of Solar Radiation Analysis using ArcGis. Bulletin UASVM Horticulture 2013; 70: 437-440.

EKİCİ BB. Variation of photovoltaic system performance due to climatic and geographical conditions in Turkey. Turkish Journal of Electrical Engineering & Computer Sciences 2016; 6: 4693-4706.

Fu P, Rich PM. The Solar Analyst 1.0 Manual. Helios Environmental Modeling Institute (HEMI), USA; 2000.

Fuentes JE, Moya FD, Montoya OD. Method for Estimating Solar Energy Potential Based on Photogrammetry from Unmanned Aerial Vehicles. Electronics 2020; 9: 2144.

Kazak JK, Swiader M. A Novel Decision Support Tool for the Assessment of Solar Radiation in ArcGIS. Energies 2018; 11: 1-12.

Kodysh JB, Omitaomu OA, Bhaduri BL, Neish BS. Methodology for estimating solar potential on multiple building rooftops for photovoltaic systems. Sustainable Cities and Society 2013; 8: 31-41.

Han Y, Pan Y, Zhao T, Wang C, Sun C. Use of UAV photogrammetry to estimate the solar energy potential buildings in severe cold region. Intelligent & Informed 2019; 2: 613-622.

Huang X, Hayashi K, Matsumoto T, Tao L, Huang Y, Tomino Y. Estimation of Rooftop Solar Power Potential by Comparing Solar Radiation Data and Remote Sensing Data - A Case Study in Aichi, Japan. Remote sensing 2022; 14: 1742.

Machete R, Falcão AP, Gomes MG, Rodrigues AM. The use of 3D GIS to analyse the influence of urban context on buildings' solar energy potential. Energy and Buildings 2018; 177: 290-302.

Ministry of Energy. Conservation of Energy in Academy Institutions. Bangkok, Thailand. 2007.

Moudrý V, Beková A, Lagner O. Evaluation of A High Resolution UAV Imagery Model for Rooftop Solar Irradiation Estimates. Remote Sensing Letters 2019; 11: 1077-1085.

Park JK, Das A, Park JH. Estimating Distribution of Precision Solar Radiation Unmanned Aerial Vehicle. IEEE Xplore 2013; 6718-6721.

Pili S, Desogus G, Melis D. A GIS tool for the calculation of solar irradiation on buildings at the urban scale, based on Italian standards. Energy and Buildings 2018; 158: 629-646.

Polo J, Bernardos A, Navarro AA, Fernandez-Peruchena CM, Ramírez L, Guisado MV, Martínez S. Solar resources and power potential mapping in Vietnam using satellite derived and GIS-based information. Energy Conversion and Management 2015; 98: 348-358.

Pop H, Grama A. Increasing Energy Efficiency Using Photovoltaic Panels. Carpathian Journal of Electronic and Computer Engineering 2021; 14(1): 6-10.

Rich PM, Dubayah R, Hetrick WA, Saving SC. Using Viewshed Models to Calculate Intercepted Solar Radiation: Applications in Ecology. American Society for Photogrammetry and Remote Sensing Technical Papers 1994; 524–529.

Rodríguez LR, Duminil E, Ramos JS, Eicker U. Assessment of the photovoltaic potential at urban level based on 3D city models: A case study and new methodological approach. Solar Energy 2017; 146: 264-275.

Suomalainen K, Wang V, Sharp B. Rooftop solar potential based on LiDAR data: Bottom-up assessment at neighbourhood level. Renewable Energy 2017; 111: 463-475.

Wong MS, Zhu R, Liu Z, Lu L, Peng J, Tang Z, Lo CH, Chan WK. Estimation of Hong Kong's solar energy potential using GIS and remote sensing technologies. Renewable Energy 2016; 99: 325-335.

Yalcin E. Generation of high-resolution digital surface models for urban flood modelling using UAV imagery. WIT transactions on ecology and the environment 2018; 357-366.

Zhong Q, Nelson JR, Tong D, Grubesic TH. A spatial optimization approach to increase the accuracy of rooftop solar energy assessments. Applied Energy 2022; 316: 119128.